ejpmr, 2020,7(10), 116-124

SJIF Impact Factor 6.222

EUROPEAN JOURNAL OF PHARMACEUTICAL AND MEDICAL RESEARCH

www.ejpmr.com

Research Article

ISSN 2394-3211

EJPMR

BIOIMPEDANCE MEASUREMENT OF SEGMENTAL FLUID VOLUMES AND HEMODYNAMICS

Leslie D. Montgomery, Ph.D.*[1], Yi-Chang Wu, M.D.[1] and Wayne A. Gerth, Ph.D.[1]

[1]LDM Associates, 1764 Emory Street, San Jose, CA 95126.

***Corresponding Author: Leslie D. Montgomery, Ph.D.**

LDM Associates, 1764 Emory Street, San Jose, CA 95126.

Article Received on 11/08/2020 **Article Revised on 01/09/2020** **Article Accepted on 21/09/2020**

ABSTRACT

Background: Bioimpedance has become a useful tool to measure changes in body fluid compartment volumes. An Electrical Impedance Spectroscopic (EIS) system is described that extends the capabilities of conventional fixed frequency impedance plethysmographic (IPG) methods to allow examination of the redistribution of fluids between the intracellular and extracellular compartments of body segments. ***Methods***: The combination of EIS and IPG techniques was evaluated in the human calf, thigh and torso segments of eight healthy men during 90 min of 6° head-down tilt (HDT). ***Results***: After 90 min HDT the calf and thigh segments significantly ($P<0.05$) lost conductive volume (8 and 4%, respectively) while the torso significantly ($P<0.05$) gained volume (approximately 3%). Hemodynamic responses calculated from pulsatile IPG data also showed a segmental pattern consistent with vascular fluid loss from the lower extremities and vascular engorgement in the torso. Lumped-parameter equivalent circuit analyses of EIS data for the calf and thigh indicated that the overall volume decreases in these segments arose from reduced extracellular volume that was not completely balanced by increased intracellular volume. ***Conclusion:*** The combined use of IPG and EIS techniques enables noninvasive tracking of multi-segment volumetric and hemodynamic responses to environmental and physiological stresses.

KEYWORDS: Bio-Impedance, Impedance Spectroscopy, Fluid redistribution, Hemodynamics, Head-down tilt, Intracellular volume, Extracellular volume

INTRODUCTION

Redistributions of body fluids between different body segments (i.e. legs, torso, and arms) and between the intra- and extracellular compartments within these segments, are important physiological features of shock and other clinical disorders[6,14] and of response and adaptation to various orthostatic and anti-orthostatic stresses, including microgravity.[3,8,10-12,15,21,22] These fluid redistributions affect cardiovascular function, water balance and perhaps skeletal muscle function[3,6,8,10] through physiological mechanisms that may be better understood with simultaneous characterization of both the fluid redistributions themselves and of associated changes in cardiovascular and hemodynamic parameters. Fixed frequency bioelectrical impedance plethysmographic (IPG) techniques have emerged as valuable noninvasive tools that provide information about overall segmental volumes and hemodynamic status.[16,20,18,28] However, these techniques cannot provide information about relative redistributions of fluids between the intra- and extracellular compartments of body segments.

Electrical impedance spectroscopy (EIS),[24] coupled with computer-aided equivalent circuit analysis, can measure such compartmental changes.[2,5,9] The combination of fixed frequency and spectroscopic bioimpedance monitoring would provide a detailed characterization of the human body's regional volume, hemodynamic, and blood flow responses to disease, proposed physiologic countermeasures, and to short term head down tilt simulation of microgravity.

Objective

The specific objective of this work is to demonstrate that combined IPG and EIS techniques can be used to measure segmental fluid volumes and hemodynamics.

METHODS

System Overview

The combined impedance system used tandem operation of separate EIS and IPG instruments. Electrical Impedance Spectroscopy The EIS system consisted of a Schlumberger Technologies, Inc. (New york, NY), Solartron 1260 Impedance/Gain-Phase Analyzer controlled via an IEEE-488 interface by a Digital Equipment Corporation (Houston, TX), VAXstation

3200 computer. The entire system (except a printer) was mounted in one full EIA standard cabinet rack on castors.

An impedance spectrum was obtained by measuring the voltage across a segment to sinusoidal electric current excitation at each of a series of discreet frequencies from 3 to 150 kHz. A signal generator and current amplifier provided the excitation signal which was passed through the segment and terminated at a current input channel, where the amplitude and phase of the current were measured. Electric response of two segments in the excitation current path was measured across independent voltage input channels. Tetrapolar electrode configurations were used to minimize electrode impedance effects. System software was used to configure the analyzer for spectrum acquisition by setting appropriate values for all analyzer functions, including the excitation current and the frequencies to be swept. The analyzer was operated in differential mode on each of its two channels with the shields for all output and input leads floated from ground at the analyzer chassis. Shields of all leads were also brought to equal potential at a single point near the electrode ends of the leads.

The excitation current was fixed at about 0.5 mA or increased as a function of frequency from about 0.3 mA to a maximum of 5.0 mA (3.0 V max). The latter procedure maximizes signal-to-noise ratios and measurement accuracy where maximum safe drive currents decrease with decreasing frequency. As the measurement frequency increased during each sweep from about 2.5 kHz to 150 kHz, the drive current was adjusted upward using the log-log relationship: lnI = mlnf + b; where: I is the current at frequency f, and values of m and b were set conservatively according to data for the frequency dependence of the threshold for current sensation in the human thorax.[7] A minimum current of 0.3 - 1.0 mA was used when this relationship gave smaller values and a limit of 5.0 mA was imposed at higher frequencies. Data were passed in binary form from the analyzer to the computer for immediate processing and storage on disk or magnetic tape.

Impedance Plethysmography A tetrapolar, multi-channel impedance plethysmograph (UFI Inc., No. 2994, Morro Bay, CA) was used to measure baseline resistances (Ro) and pulsatile resistance changes (ΔR) in each monitored body segment. The IPG operated at a constant current, fixed excitation frequency of 50 kHz (0.1 mA, rms). A UFI Cardiotach (Morro Bay, CA) was used to monitor a lead I electrocardiogram (ECG). The seven analog outputs (6 impedance, 1 ECG) were each sampled at 200 Hz and recorded in digital form using a IBM-compatible personal computer with an 8-channel differential A/D convertor (Data Translation, Inc., DT-2811L, Marlboro, MA) running under control of a commercially available high-speed data acquisition system (DataQ, Inc., CODAS, Akron, OH).

System Data Acquisition

Each EIS impedance spectrum consisted of a series of discreet impedances (Z*) computed from the measured voltage V* and current I* at each of the separate frequencies in the sweep, where:

$$Z^* = V^*/I^* = R + Xj \; ; \qquad (1)$$

where $j = \sqrt{-1}$ and R is the equivalent series resistance and X is the equivalent series reactance.

A simple lumped-parameter equivalent circuit model representing idealized conductance paths through the body segment was fitted to each measured spectrum using a nonlinear least squares routine based on Marquardt's algorithm. [17] The circuit (Figure 1) models the segment as a uniform isotropic bidomain conductor[23] with an extracellular compartment having

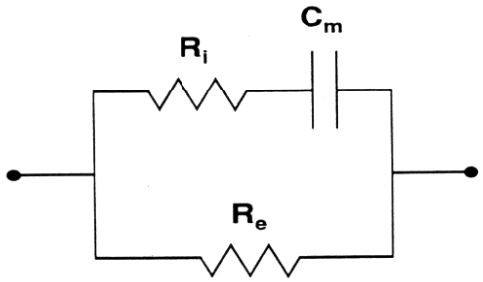

Figure: 1. Equivalent circuit used to interpret measured segmental impedance spectra.

average resistance Re, and an intracellular compartment having average resistance Ri and average capacitance Cm. The value of Ri is governed by both membrane and cytoplasmic properties, while Cm is governed principally by membrane properties.[1] The complex admittance Y* of the circuit is given by

$$Y^* = \frac{1}{Z^*} = \frac{1}{Re} + \frac{1}{Ri - \frac{1/Ri}{1 + j\omega\tau^{\circ\,(1-\alpha)}}} \; , \quad 0 < \alpha < 1 \; ; \qquad (2)$$

where: ω is the angular frequency given by 2πf, τ° is the time constant given by the product Ri·Cm, and απ/2 is the angle between the real axis and a radius of the admittance locus passing through either of its two real axis intercepts. The (1-α) exponent in Eq. (2) is included to account for the typical failure of tissue impedance loci to be centered on the real axis. This behavior is consistent with the presence in tissue of a practical infinitude of parallel R-C elements each with different time constants with values distributed about a mean at τ°.[1,4,13] By definition, α=0 when the center of the locus lies on the real axis. Increasing values of α from 0 towards unity indicate a widening of the distribution of time constants with increasing standard deviation of the distribution about τ°.

Marquardt's algorithm was implemented using the norm of each observed impedance $|Z^*|$, and that of the corresponding fitted impedance $|\not{Z}^*|$. The algorithm adjusted the model parameters to minimize the sum of squares, (SS),

$$SS = \sum_{i=1}^{n} \{ |Zi^*| - |\not{Z}i^*| \}^2, \qquad (3)$$

for the impedances at the n different frequencies in each spectrum. The analytic components of the software were bundled to process run-time data passed from the impedance spectrum acquisition routine, or to read and process data files from earlier experiments thus providing identical output in either case. In the former mode the analyses were performed immediately after acquisition of each spectrum. Graphic display of the results afforded a means to track changes in measured and computed dielectric properties of each body segment throughout each run.

Impedance plethysmographic data were analyzed on a pulse-by-pulse basis using a custom interactive software package[19] that included a graphic user interface to facilitate selection and specification of the impedance waveform landmarks shown in Figure 2. Times and differential resistances at these landmarks were used with basal resistances to calculate the following indices of segmental volume, blood flow and vascular compliance:

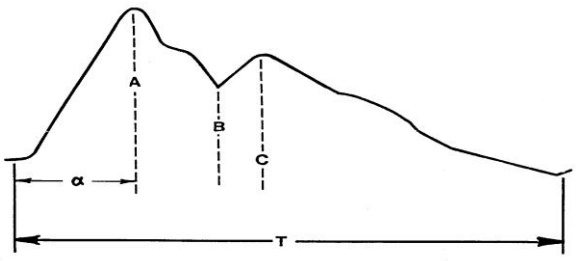

Figure: 2. Impedance plethysmographic pulse waveform with landmarks for calculation of hemodynamic parameters.

(1) segmental conductive volumes (Ve) were calculated from segmental base resistances;[18]

(2) blood flow index, (BFI) is a function of the maximum amplitude of the impedance pulse, heart rate, and the basal resistance;[20]

(3) dicrotic index, (DCI) = B/A and is defined as the ratio of the amplitude of the pulse waveform at the height of the incisure (B) to the maximum pulse amplitude (A). DCI increases proportionally with general arteriolar compliance:[28]

(4) anacrotic index, (AI) = α /T and is defined as the ratio of the duration of the anacrotic phase of the pulse wave (α) to the duration of the entire cardiac cycle (T). This ratio is the relative systolic filling time of a given body segment during the cardiac cycle and reflects the compliance of the larger arteriolar vessels. AI decreases as the local arteriolar compliance increases, and

(5) pulse transit time (PTT) is the time interval in seconds between the onset of the ECG QRS complex and the onset of the impedance pulse waveform; i.e. the time required for the pressure profile of the cardiac pulse to be transmitted from the heart to the monitored segment. As the pulse conduction path becomes more rigid the pressure pulse is transmitted more quickly. Thus, PTT is an index of the overall vascular compliance of the body.[26]

Subject Testing Procedure

Eight men (27 to 50 yrs) in good health provided informed consent and volunteered for the 90 min 6° head-down tilt (HDT) protocol. The investigation took place in the F.G. Hall Hypo/Hyperbaric Laboratory in the Duke University Medicine Center and was fully approved by the Human Use Committees of both SRI International, Menlo Park, CA and Duke University Medical Center. Each test sequence consisted of three successive periods when the subject was in the seated upright for 30 min, supine at 6° head-down tilt for 90 min, and again then seated upright for 60 min. Except for standing to move from one position to the next, the subject was at rest and asked to minimize limb movement and muscle contraction throughout each run conducted at 21.0 ± 0.5°C average ambient temperature where air movement, bright light, noise, and other stimulation were minimized. All subject data was recorded in such a way that the individual subjects could not be identified by their data.

Each subject was fitted with ECG electrodes (3M, Ag/AgCl Red Dot, St. Paul, MN) for bioimpedance monitoring of the left calf, thigh and torso. Calf pickup electrodes were placed laterally above the lateral malleolus of the fibula and below the fibular head. Thigh pickup electrodes were placed just above the lateral epicondyle of the femur and on the lateral aspect of the greater trochanter of the femur. Torso pickup electrodes were placed on the left iliac crest and the left clavicular line. Distances between the pickup electrodes for each segment were measured for calculation of segmental conductive volumes.[18] Drive electrodes were placed on the dorsum of the metatarsus and on the lateral aspect of the anterior superior iliac spine. An electrode on the back of the left hand was used in place of the latter for IPG monitoring to include the torso in the current path. Each subject was also instrumented with standard sternal and biaxillary ECG electrodes for monitoring heart rate.

EIS was used at five min intervals to characterize the dielectric properties of each body segment. Data acquisition for each impedance spectrum required about 70 s and measured 50 discreet frequencies distributed

logarithmically from 3 to 150 kHz. At run elapsed times of 0, 40, 65, 115, 130 and 185 min. The electrodes were disconnected from the EIS system and connected to the IPG system. Two-minute periods of IPG measurements of baseline resistance (Ro) and pulsatile resistance changes (ΔR) were then made of the calf, thigh, and torso body segments.

Statistical Analysis

Data were analyzed with the paired-t test of measured and calculated parameters.

RESULTS

Calf, thigh and torso conductive volume changes during the HDT period are shown in percent relative to the first value obtained after start of the HDT period; i.e., the value obtained at 40 min total elapsed time or 8-10 min after initial assumption of the HDT position (Figure 3).

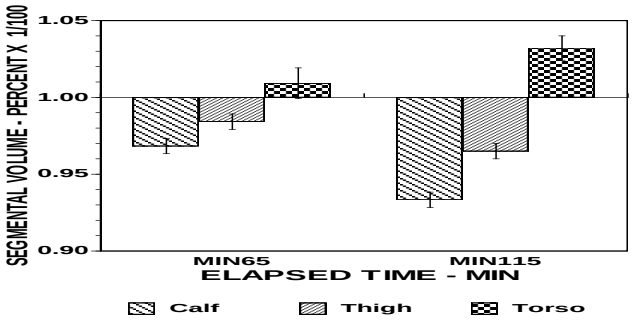

Figure: 3. Grouped mean segmental conductive volumes vs elapsed time. An asterisk (*) indicates that the value differs significantly (P<0.05) from the initial head-down tilt value. A plus (+) indicates that the value differs significantly (P<0.05) from that at 65 min elapsed time.

By minute 65 (approximately 33 min HDT), the calf segment had lost approximately 3% of its conductive volume (P<0.05), the thigh had lost about 2% volume and the torso had gained about 1.5% volume. After 90 min HDT, the volumes of all three body segments had changed significantly (P<0.05) relative to the first measurement during HDT. The calf and thigh had lost approximately 8 and 4% volume, respectively, and the torso volume had increased by approximately 3%.

An impedance spectrum is visualized as a locus of points in the complex plane by plotting the imaginary vs the real parts of the impedance (reactance vs resistance) at each frequency in the spectrum. Impedance loci of the calf and thigh of one subject at the end of each of the three periods in the test protocol are shown in Figure 4. Typifying the results for all

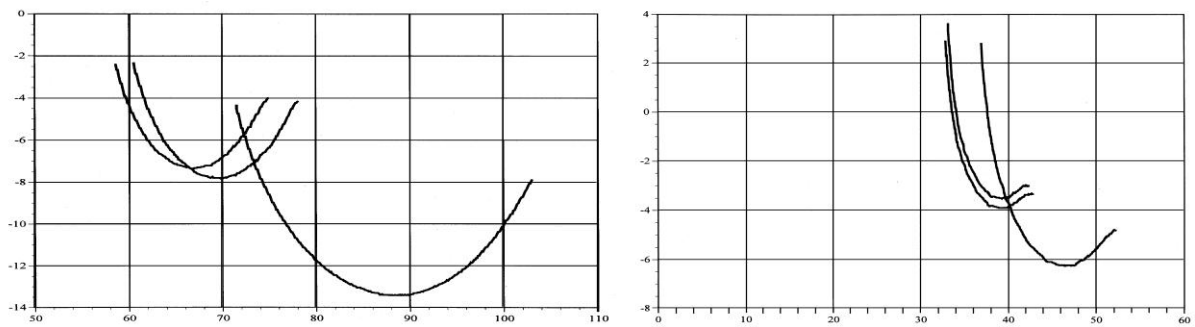

(A) **(B)**

Figure: 4. Complex impedance loci of one subject's: (A) calf and (B) thigh at (a) the end of the pre-tilt seated period; (b) after 90 min HDT, and; (c) at the end of the 30 min seated recovery period. Each locus consists of points from measurements at 50 discreet frequencies from 3 to 150 kHz. Individual points are obscurred by connecting straight lines. The lowest frequency impedance is at the right-most or highest resistance end of each locus.

subjects, the loci were widened and shifted towards higher R and more negative X values at the end of the HDT period in both segments. At the end of the post-tilt period, the locus for each segment resembled that obtained at the end of the pre-tilt period.

Grouped mean values of the fitted equivalent circuit parameters for the calf and thigh at the various elapsed times in the protocol are shown in "strip chart" format in Figure 5. Both the

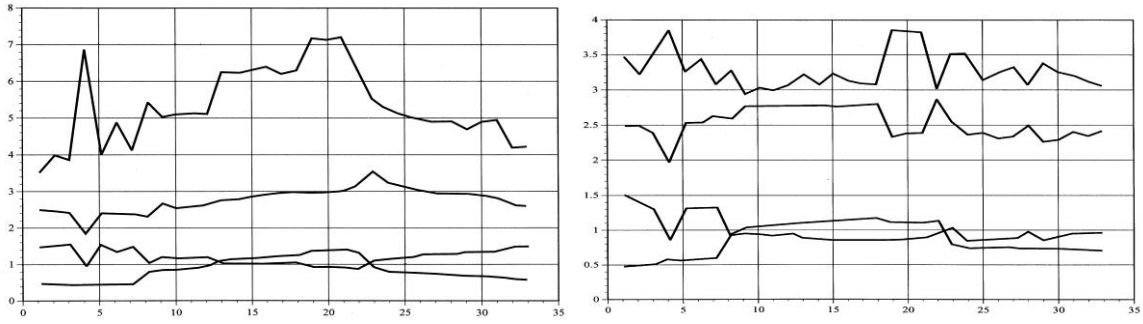

(A) **(B)**

Figure: 5. Grouped mean values of fitted equivalent circuit parameters vs run elapsed time for: (A) the left calf, and; (B) the left thigh of the four subjects in the study. Parameter values are shown in "strip chart" format, with the ordinate scaled such that the major ticks above and below the first value shown at t=0 represent + and - 20% deviation, respectively, from that value. Re and Ri are in Ohms, Cm is in micro-farads and a is dimensionless.

amplitudes and the time courses of the parametric changes during HDT followed somewhat different patterns in the two segments. In both segments, the Re and Ri parameters showed large rapid changes at the outset of HDT that were not evident in the behavior of the Cm parameter. The tendencies for the resistance parameters to continue changing and for Cm to increase throughout the remaining period of HDT was more pronounced in the calf than in the thigh. At the end of the HDT period, mean calf Re values had increased 35%, mean calf Ri values had decreased 24% and mean calf Cm values had increased 33% from their values at the end of the pre-tilt period. Parametric changes in the thigh were similar but attenuated. Mean thigh Re increased 26%, mean thigh Ri decreased 14% and mean thigh Cm increased 12% over the same interval.

The magnitudes of the above Re and Ri changes during HDT substantially exceeded those for the corresponding segmental conductive volume changes in Figure 3. These two sets of results are properly compared, however, only after reducing the Re and Ri parameter pairs from each impedance spectrum to a mutual resistance, Rm, using the parallel relation: Rm = 1/(1/Re + 1/Ri). Changes in resultant Rm values during HDT then show excellent agreement with those in calculated segmental conductive volumes. For example, over the interval in Figure 3 spanned by the results at an elapsed time of 115 min, calf and thigh Rm increased 9 and 5%, respectively, compared to the 8 and 4% changes in respective conductive volumes.

Figures 6 and 7 present the grouped mean values (± S.E.) of the calculated segmental hemodynamic indices at the indicated elapsed times during the test protocol. Results are shown normalized and reduced to percent parametric change for each segment relative to the initial pre-tilt value (@ t=0).

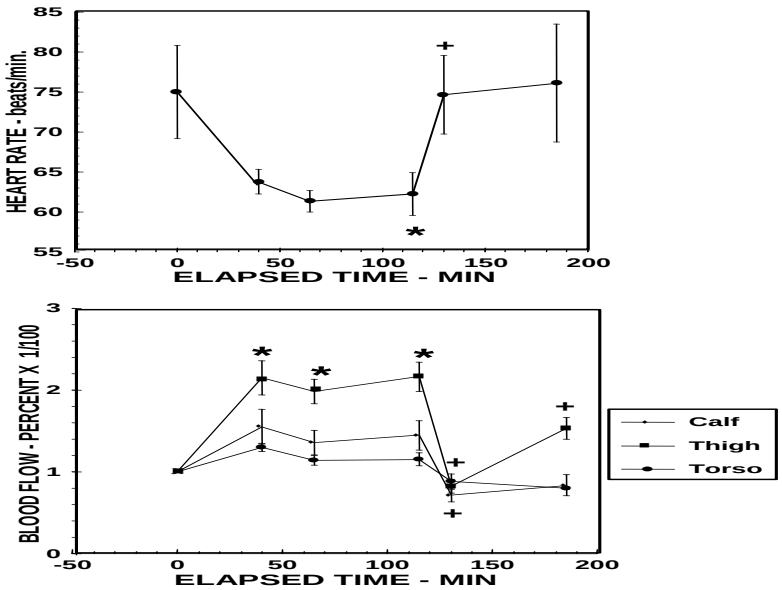

Figure: 6. Grouped mean heart rates (A-top panel) and blood flow indices (B-bottom panel) vs elapsed time. An asterisk (*) indicates that the value differs significantly (P<0.05) from that during the pre-tilt seated position. A plus (+) indicates that the value differs significantly (P<0.05) from the preceding value.

The grouped mean heart rate (Figure 6A) decreased approximately 10% (P<0.05) during the HDT period, and returned to pre-tilt values within minutes of assuming the seated recovery position. The blood flow indices of the calf, thigh, and torso segments all increased (P<0.05) (Figure 6B) during the first 30 minutes of HDT, 50, 115 and 30% respectively. After 90 min HDT, the index for the thigh segment remained elevated, while indices for the calf and torso showed respectively greater tendencies to decrease toward their pre-tilt values.

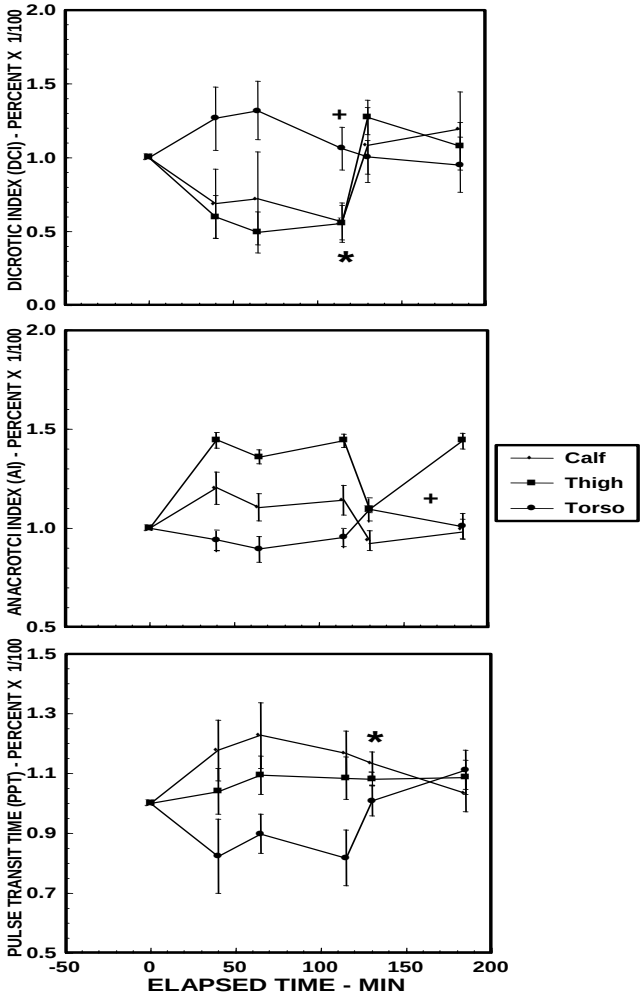

Figure: 7. Grouped mean segmental dicrotic indices (A-top panel), anacrotic indices (B-middle panel), and Pulse transit times (C-bottom panel) vs elapsed time. An asterisk (*) indicates that the value differs significantly (P<0.05) from that during the pre-tilt seated position. A plus (+) indicates that the value differs significantly (P<0.05) from the preceding value.

The dicrotic index (Figure 7A) decreased (P<0.05) in the calf and thigh throughout the HDT period. In contrast, this index for the torso increased (P<0.05) during the first 30 min of HDT and decreased (P<0.05) to its pre-tilt value after 90 min HDT. The anacrotic index (Figure 7B) increased (P<0.05) between 20 and 40% in the calf and thigh but decreased (P<0.05) approximately 10% in the torso during HDT. Finally, segmental pulse transit times (Figure 7C) increased (P<0.05) in the lower body segments and decreased (P<0.05) in the torso during the HDT period. Changes in each of these separate segmental hemodynamic indices indicate that vascular compliance increased in the calf and thigh but decreased in the torso during HDT.

DISCUSSION

Results provide a detailed multi-segmental description of the volumetric and hemodynamic changes that occur during the initial 90 min of anti-orthostatic bed rest. This environmental stressor is widely used to simulate the cardiovascular effects of microgravity and has known effects on fluid distribution and cardiovascular performance.[3,10,12,13,16] In conformance with these known effects, cardiovascular, hemodynamic and volumetric parameters provided by the present techniques exhibited systematic and dynamic changes during HDT that were reversible and showed patterns among the monitored segments that varied in accord with the orthostatic dependence of the segments. More generally, this study demonstrates the broad scope of information that comprehensive applications of

impedance spectroscopic and plethysmographic techniques can provide in other experimental contexts as well.

The IPG results indicate that the calf and thigh segments lost conductive volume while the torso gained volume during HDT. This pattern is typical of a general cephalad shift of fluids, where the volume gain in the torso represents a portion of the fluid displaced from the lower segments. Observed segmental volume changes are consistent with those determined in a similar fashion in other studies and shown to agree well with the volume changes determined from simultaneous anthropometric, capacitance band and strain-gauge plethysmographic measurements.[18] The agreement between the changes in mutual resistance calculated from the EIS results and the changes in segmental conductive volumes determined from the IPG data thus provides an important cross-validation of the two techniques: The segmental fluid shifts evident in the IPG results are also evident in the EIS results.

Significantly, the EIS results provide additional insights into how the segmental intra- and extracellular compartments participate in the fluid shifts. Because the equivalent circuit model as presently applied ignores the inequalities of the transverse and longitudinal resistivities of muscle masses in the monitored segments, calculated compartmental resistance and capacitance values have only limited absolute significance.[18] However, for a given electrode orientation, fractional changes in these values, as presented in Figure 5, accurately reflect actual changes in compartmental properties, provided that the processes leading to such changes uniformly affect all the monitored tissue. Thus, with assumption and maintenance of the HDT position, large initial increases in both calf and thigh Re reflect the exsanguination of capacitance vessels, while the more gradual increases in these parameters continuing throughout HDT indicate interstitial fluid loss. The latter was more pronounced in the calf than in the thigh, indicating, in accord with the different antiorthostatic stresses in the segments, that interstitial fluid loss in the thigh was small compared to that in the calf. These results are consistent with previously reported decreases of interstitial and transcapillary pressures in the calf soleus muscle that continued throughout 8 hr of 5° HDT.[10] Upon resumption of the seated position, the fluid movement pattern reversed, with rapid return of the vascular volume in both segments followed by a gradual recovery of the respective interstitial volumes.

Changes in the Ri and Cm parameters illuminate changes in the volumes and ionic concentrations of the segmental intracellular spaces. The decreases in calf Ri that accompanied assumption and maintenance of the HDT position indicate that the average volume and/or electrolyte concentration of the intracellular space increased. The former interpretation is supported by the observed coincident increases of calf Cm. Increases in this parameter are plausibly interpreted to arise from decreases in the segmental average cell membrane thickness and increases in membrane area, such as would accompany increases in average cell volume. The indication that cells in the calf swell when the body is under anti-orthostatic stress is in accord with evidence that calf interstitial osmotic pressure decreases during HDT.[10] Similar but attenuated indications were obtained for the compartmental responses in the thigh.

The EIS results consequently augment the IPG results by providing evidence that HDT-induced losses of conductive volume from the calf and thigh arise from rather large losses of extracellular fluid that are not completely balanced by cellular imbibition of fluid. Similar conclusions have been forwarded by other workers for humans during chair rest and water immersion, where significant decreases of serum osmolality were observed,[8] and during horizontal bed rest.[11] Hargens, et al.,[10] also reported increases of cellular area in connective tissue of soleus muscle biopsied from human subjects after 8 hr HDT, although a net intracellular to extracellular fluid shift -- opposite that presently indicated -- was concluded to have occurred on the basis of increased potassium and decreased creatinine urinary excretion. It is of interest that decreases of serum osmolality, the most probable cause of intracellular fluid accummulation, evidently occur in astronauts during spaceflight.[15] Notwithstanding the controversy about the direction of compartmental fluid shifts induced by anti-orthostasis, the presently indicated shifts are surprisingly large. The relative diminution of the shifts in the thigh with respect to those in the calf suggest that the net whole-body shift must be smaller, but the mechanism for such segmental differentiation is unknown. Further validation of the method is required to etermine to what extent the effects might be quantitatively overestimated as a result of nonuniformities of current flow in the monitored segments and changes therein that could be caused by changes in the relative fluid contents of the composite tissues.

As observed for the segmental volumetric responses, the hemodynamic parameters calculated from the pulsatile IPG data also showed segment-specific responses to changes in orthostatic stress. Both the calf and thigh manifested hemodynamic responses to HDT that would have tended to minimize intravascular fluid loss from those segments. Decreases in the dicrotic index, and increases in the anacrotic index and pulse transit time indicate that the overall calf and thigh vascular compliance increased during HDT. These changes tended to be more pronounced in the calf than in the thigh, reflecting the same orthostatic dependence evident in the segmental fluid shifts. Conversely, hemodynamic parameters in the torso exhibited changes during HDT that would have tended to minimize vascular

engorgement in this segment. Thus, segmental hemodynamic changes during HDT appear to have been coordinated to limit or reduce the transfer of intravascular fluid from the legs to the torso and head. This counterregulatory pattern is consistent with that found by other investigators in human subjects under similar anti-orthostatic stresses,[12,16,25] and probably arises from both active changes in arteriolar tone and passive volume-related changes in compliance.

Segmental blood flow changes during HDT were generally consistent with the indicated changes in vascular compliance, reflecting the overall efficacy of the latter at redistributing an increased central venous return. Blood flow increased and remained elevated in the thigh during the HDT period. It should be noted that these flows include throughput for perfusion of the calf, where flow was also increased. Blood flow in the torso increased at the beginning of HDT, but tended to decrease toward the pre-tilt value during the latter stages of HDT. Heart rate determined from the ECG remained decreased throughout HDT. Given the increased torso blood flow, this result indicates that cardiac stroke volume increased during HDT. Results are generally in accord with earlier indications that cephalad shifts of blood during HDT cause increased end-diastolic volume and cardiac output, with the latter causing segmental blood flow increases.[3,21,22] The presently observed tendency for return of the cardiovascular parameters to pre-tilt values after an initial HDT-induced transient is also consistent with results of other studies, although the present time course for such adaptation appears longer than in other work.[3]

CONCLUSIONS

The combination of fixed and swept frequency bioimpedance monitoring has provided a detailed characterization of the human body's regional volume, hemodynamic and blood flow responses to a short term head-down tilt simulation of microgravity. Observed responses are within the ranges of those reported from other studies, while regional patterns of the responses indicate that studies of this type should include examination of the relevant parameters to at least the segmental level of anatomic resolution. The present techniques provide such resolution augmented by a high level of temporal resolution using only simple superficial electrodes. Occlusion cuffs, displacement fluids, confining garments or invasive procedures are not required, making the methods suitable for applications under either laboratory or field operational conditions. These techniques afford a useful noninvasive means to monitor a variety of physiological parameters central to the physiology of fluid control in aerospace and clinical environments.

ACKNOWLEDGEMENT

This research was supported in part by a contract from the U.S. Navy Bureau of Medicine, Contract No. N00014-87-C-0166.

REFERENCES

1. Ackmann JJ, Seitz MA. Methods of complex impedance measurement in biologic tissue. CRC Critical Reviews in Biomedical Engineering, 1984; 11: 281-311.
2. Baarends EM, VanMarken Lichtenbelt WD, Wouters EFM, Schols AMWJ. Body-water compartments measured by bio-electrical impedance spectroscopy in patients with chronic obstructive pulmonary disease. Clincial Nutrition, 1998; 17: 15 - 22.
3. Butler GC, Xing H, Hughson RL. Cardiovascular response to 4 hours of 6° head-down tilt or of 30° head-up tilt bed rest. Aviat. Space Environ. Med, 1990; 61: 240-6.
4. Cole KS, Cole RH. Dispersion and absorption in dielectrics. I. Alternating current characteristics. J. Chem. Phys, 1941; 9: 341-52.
5. Cox-Reijven PL, Soeters PB. Validation of bio-impedance spectroscopy: Effects of degree of obesity and ways of calculating volumes from measured resistance values. Int. J. Obesity, 2000; 24: 271 - 280.
6. Gauer OH, Henry JP, Behn C. The regulation of extracellular fluid volume. Ann. Rev. Physiol, 1970; 32: 547-95.
7. Geddes LA, Baker LE. Hazards in the use of low frequencies for the measurement of physiological events by impedance. Med. & Biol. Engng, 1969; 7: 289-96.
8. Greenleaf JE, Shavartz E, Kravik S, Keil LC. Fluid shifts and endocrine responses during chair rest and water immersion in man. J. Appl. Physiol.: Respirat. Environ. Exercise Physiol, 1980; 48(1): 79-88.
9. Gotshall RW, Davrath LR. Bioelectric impedance as an index of thoracic fluid. Aviat. Space Environ. Med, 1999; 70: 58 - 61.
10. Hargens AR, Tipton CM, Gollnick PD, Mubarak SJ, Tucker BJ, Akeson WH. Fluid shifts and muscle function in humans during acute simulated weightlessness. J. Appl. Physiol.: Respirat. Environ. Exercise Physiol, 1983; 54(4): 1003-9.
11. Johnson PC, Driscoll TB, Carpentier WR. Vascular and extravascular fluid changes during six days of bedrest. Aerospace Med, 1971; 42(8): 875-8.
12. Kabesheva TA, Kopanev SV, Panfervoa NY, Zavadovshiy AF. Vascular mechanisms of adaptation to antiorthstatic position. Kosmich. Biol. Aviak. Med, 1985; 19(2): 35-9.
13. Kanai H, Katsuyuki S, Haeno M. Electrical measurement of fluid distribution in human legs: Estimation of extra- and intracellular fluid volume. J. Microwave Power, 1983; 18: 233-43.

14. Klassen P, Mazariegos M, Deurenberg P, Solomons NW, Furst P. Hydration status assessed by bioelectrical impedance spectroscopy and dilution methods in patients with classical dengue fever. In Yasumura S, Wang J, Pierson Jr. RN (Eds). In vivo body composition studies. Ann. NY Acad. Sciences, 2000; 904: 163 - 170.
15. Leach CS. Fluid control mechanisms in weightlessness. Aviat. Space Environ. Med, 1987; 58(9,Suppl.): 74-9.
16. Maksimov DG, Domracheva MV. Changes in central and peripheral hemodynamics during prolonged anti-orthostatic hypokinesisa as weightlessness models. Kosmich. Biol. Aviak. Med, 1976; 5: 52-7.
17. Marquardt DW. An algorithm for least-squares estimation of nonlinear parameters. J. Soc. Indust. Appl. Math, 1963; 11: 431-41.
18. Montgomery LD. Body volume changes during simulated weightlessness: An overview. Aviat. Space Environ. Med., 1987; 58(9,Suppl.): 80-5.
19. Montgomery LD, Guisado R. Rheoencephalographic and electroencephalographic measures of cognitive workload: Analytical procedures. Biological Psychology, 1995; 40: 143-159.
20. Montgomery LD, Hanish HM, Marker RA. An impedance device for study of multisegmental hemodynamic changes during orthostatic stress. Aviat. Space Environ. Med, 1989; 60: 116-22.
21. Nicogossian AE, Parker Jr. JF. Space physiology and medicine. National Aeronautics and Space Administration, 1982; 447:141-52.
22. Nixon JV, Murray RG, Bryant C, Johnson Jr. RL, Mitchell JH, Holland OB, Gomez-Sanchez C, Vergne-Marini P, Blomquist CG. Early cardiovascular adaptation to simulated zero gravity. J. Appl. Physiol.: Respirat. Environ. Exercise Physiol, 1979; 46(3): 541-8.
23. Plonsey R, Barr RC. A critique of impedance measurements in cardiac tissue. Annals of Biomed. Engng, 1986; 14: 307-22.
24. Siconolfi SF, Gretebeck RJ, Wong WW, Pietrzyk RA, Suire SS. Assessing total body and extracellular water from bioelectrical response spectroscopy. J. Appl. Physiol, 1997; 82(2): 704 - 710.
25. Skagen K. Sympathetic reflex control of blood flow in human subcutaneous tissue during orthostatic maneuvers. Danish Medical Bulletin, 1983; 30(4): 229-41.
26. Strandness DE, Sumner DS. Hemodynamics for Surgeons. New York: Grune and Stratton, 1975; 187-96.
27. Usochev VV, Shinkarevskaya IP. Functional changes in systemic and regional (intracranial) circulation accompanying low acceleration. Kosmich. Biol. Aviak. Med, 1973; 19(1): 59-64.
28. Yarullin KK, Krupina TN, Vasil'yeva TD, Buyvolova NN. Changes in cerebral, pulmonary, and peripheral blood circulation. Kosmich. Biol. Aviak. Med, 1972; 6(4): 33-9.